International Journal of Applied Earth Observation and Geoinformation 118 (2023) 103241

Contents lists available at ScienceDirect

International Journal of Applied Earth Observation and Geoinformation

journal homepage: www.elsevier.com/locate/jag

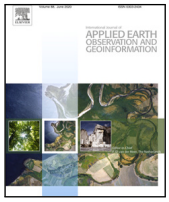

Coherency and phase delay analyses between land cover and climate across Italy via the least-squares wavelet software

Ebrahim Ghaderpour *, Paolo Mazzanti, Gabriele Scarascia Mugnozza, Francesca Bozzano

Department of Earth Sciences & CERI Research Centre, Sapienza University of Rome, P.le Aldo Moro, 5, Rome, 00185, Italy
NHAZCA s.r.l., Spin-off Sapienza University of Rome, Via Vittorio Bachelet, 12, Rome, 00185, Italy

ARTICLE INFO

Keywords:
Coherency
Ecoregion
Land cover
LST
LSWAVE
MODIS
NDVI
Phase delay
Precipitation
Trend

ABSTRACT

Land cover and climate monitoring is a crucial task in agriculture, forestry, hazard management, and ecosystems assessment. In this paper, normalized difference vegetation index (NDVI), land surface temperature (LST), and land cover products by the moderate resolution imaging spectroradiometer (MODIS) as well as precipitation were utilized to monitor the spatiotemporal dynamics of vegetation and climate along with their correlation and coherency across Italy during 2000–2021. The analyses were performed on both pixel and ecoregion levels via the least-squares wavelet software (LSWAVE). It was found that relatively more areas in all ecoregions had positive NDVI gradients than negative for each month since 2000. It was estimated that the average NDVI has increased by ~0.07 since 2000 for all ecoregions. Except the southern ecoregion which showed an insignificant daytime cooling, other ecoregions have been warming by less than 0.05 °C/year since 2000. Furthermore, precipitation had an insignificant decreasing trend for almost all ecoregions over the past two decades. The annual coherency between NDVI and LST was found much stronger than the annual coherency between NDVI and precipitation. The annual cycles of NDVI and LST were out-of-phase for the southern ecoregion while the annual cycle of precipitation led the one in NDVI by about one month for this ecoregion, the only ecoregion showing the highest Pearson correlation (53%) and annual coherency (39%) between NDVI and precipitation. For other ecoregions, the annual cycles of NDVI and LST were approximately in-phase, i.e., less than a month phase delay.

1. Introduction

Vegetation plays a vital role in keeping the climate stable through transpiration and carbon cycle regulation, and it is an essential substance between the atmosphere, water, and soil (Zhang et al., 2017; Ghorbanian et al., 2022). During photosynthesis, vegetation consumes carbon dioxide which can slightly mitigate the effect of anthropogenic carbon emissions, and it is a key component for attenuating climate change in the future (Forzieri et al., 2022). Many factors can directly or indirectly affect vegetation, such as climate change, anthropogenic activities, wildfires, and landslides (Ghorbanian et al., 2022). For example, the land surface temperature along with sunlight and soil moisture can determine whether the land supports vegetation. On the other hand, vegetations through evapotranspiration and shades can cool down the land (Alexander, 2021; Shawky et al., 2023). Understanding the interconnection between vegetation and climate is essential for management strategies to maintain a sustainable environment in the face of climate change (Tomlinson et al., 2011).

The moderate resolution imaging spectroradiometer (MODIS) is a reliable sensor onboard Terra and Aqua satellites, providing Earth and climate data for over two decades. The MODIS normalized difference vegetation index (NDVI) is a simple yet effective index that is sensitive to chlorophyll concentrations and widely applied to many research areas, such as drought monitoring, climate change, agriculture, and forestry (Touhami et al., 2022). Trend and change detection analyses have been performed on MODIS NDVI in various studies. Ghorbanian et al. (2022) estimated linear and non-linear trends for MODIS NDVI time series (250 m) across Iran. Wang et al. (2019) performed several regression analysis methods to investigate changes in MODIS NDVI time series for Shiyang River Basin.

The MODIS land surface temperature (LST) and MODIS land cover data have also been employed in conjunction with MODIS NDVI in several studies. Neinavaz et al. (2020) employed artificial neural networks to investigate the relationships between NDVI and LST for agriculture and forest ecosystems. Abdulmana et al. (2021) performed trend analysis and investigated the relationships between these datasets for Taiwan from 2000 to 2020 via multivariate linear regression. They observed a stronger correlation between NDVI and LST over vegetated lands than

* Corresponding author.
E-mail address: ebrahim.ghaderpour@uniroma1.it (E. Ghaderpour).

https://doi.org/10.1016/j.jag.2023.103241
Received 1 January 2023; Received in revised form 14 February 2023; Accepted 20 February 2023
Available online 28 February 2023

over built-up regions. Yan et al. (2020) processed MODIS monthly LST data for 2002–2018 in North America and found that North America was warming during this period by ~0.02 °C/year. Son et al. (2012) utilized a decade of MODIS data to monitor agricultural drought in the Lower Mekong Basin in Asia during dry seasons. Since cloud contamination removes many daily and 8-day pixels of the MODIS LST products, they employed the monthly MODIS LST data and found it suitable for agricultural drought monitoring. Song et al. (2021) analysed trends in MODIS LST across China from 2003 to 2019 via linear and non-linear regression models and showed that vegetation and air temperature were the main influential factors of LST dynamics.

Global precipitation measurement (GPM) is an international satellite mission operated by the National Aeronautics and Space Administration (NASA) which provides next generation precipitation observations globally (Huffman et al., 2017). The GPM satellite is an advanced successor to the Tropical Rainfall Measuring Mission (TRMM) which has additional channels, namely, the dual-frequency precipitation radar, and the GPM microwave imager, able to sense snow and light rain (Skofronick-Jackson et al., 2017). The GPM data have been used and assessed in many studies (Mahmoud et al., 2018; Shawky et al., 2019). Herein, the monthly GPM level 3 data, recommended to use for research, are utilized in addition to the MODIS products.

Not much scientific research has been published on the interconnection between vegetation and climate in Italy. Sciortino et al. (2020) estimated land productivity trends for Italy at 95% confidence level utilizing 16 years of MODIS NDVI data (2000–2016). Sarvia et al. (2021) explored the impact of climate change on vegetation phenology in the Piemonte region in Italy via MODID-NDVI data at 250 m during 2001–2019. They demonstrated that forested regions and vineyards without irrigation had more sensitivity to climate change than agricultural lands with an intense management (e.g., applying fertilizers and irrigation). Capodici et al. (2020) found a negative correlation between 12-year long MODIS NDVI and LST time series for the Imera Meridionale basin in Sicily, Italy. Negative correlations between NDVI and LST were also reported for other regions (Deng et al., 2018; Lai et al., 2020).

Linear regression is a simple and widely used method for investigating whether there is a significant trend in data (Song et al., 2021). Pearson correlation coefficient (r) is a widely used statistical metric showing the level of linear dependency between two variables (Lee Rodgers and Nicewander, 1988). However, in climate and environmental studies, researchers often need to analyse time series that contain seasonal cycles due to the tilted Earth's spin axis and other factors. Therefore, the traditional linear regression models are not recommended for estimating trends in such time series because the trend results may be easily biased by seasonal fluctuations, particularly when the time series are irregularly sampled or have missing values. The anti-leakage least-squares spectral analysis (ALLSSA) is a robust method for simultaneous estimation of harmonics and trend components in a time series which may not be evenly sampled (Ghaderpour et al., 2021).

Time–frequency analysis methods, such as wavelet and cross-wavelet analyses have been widely used for monitoring climate and vegetation. Time–frequency decomposition of time series can show how the inter- and intra-annual cycles of time series change over time (Ghaderpour et al., 2018). For example, Lian et al. (2022) utilized the cross-wavelet transform (XWT) and wavelet coherence (Torrence and Compo, 1998) to investigate spatiotemporal impacts of climate on vegetation in China using MODIS data from 2000 to 2020. Moreira et al. (2019) estimated the coherency and phase difference between vegetation and meteorological data for a southern part of Brazil and observed strong annual coherency between vegetation and temperature for all grassland types.

To study coherency and phase delay between wavelike components in multiple time series whose measurement errors may be available and possibly have different sampling rates, Ghaderpour et al. (2018) proposed two methods, the least-squares cross-spectral analysis (LSCSA) and its extension, the least-squares cross-wavelet analysis (LSCWA). Unlike XWT and wavelet coherence, LSCWA does not have the limitation of evenly sampled time series whose time indices exactly match. In addition, LSCWA can consider the observational uncertainties and provide higher time–frequency resolution cross-spectrograms (Ghaderpour et al., 2021). The ALLSSA, LSCSA, and LSCWA are the main tools of the least-squares wavelet (LSWAVE) software, developed in MATLAB and python (Ghaderpour and Pagiatakis, 2019; Ghaderpour, 2021). These tools have been used in many studies, such as trend, time–frequency, and coherency analyses of climate, streamflow, and vegetation (Ghaderpour et al., 2021; Dastour et al., 2022).

In this study, 16-day MODIS NDVI (250 m), monthly MODIS LST (~5.5 km), and monthly GPM precipitation data (~11 km) during 2000–2021 for Italy were analysed at both pixel and ecoregion levels via the LSWAVE software to estimate trends, coherency, and phase delay. The main contributions of this work are:

(a) Illustrating monthly NDVI, LST, and precipitation change maps of Italy and describing how the vegetation and climate have changed across Italy on monthly scales since 2000.

(b) Estimating the season-trend components of NDVI, LST, and precipitation at both pixel and ecoregion levels and showing their coherency and phase delays using the LSWAVE software.

(c) Demonstrating the dynamics of annual land cover classes for each ecoregion and discussing their interconnection with the dynamics of NDVI and climate.

2. Materials and methods

2.1. Study area

Italy is heavily rich in biodiversity due to its wide range of biogeographic regions and climate and is an interesting region for studying and assessing vegetation and climate dynamics. However, there is a significant lack of knowledge between climate-induced vegetation and land cover changes throughout Italy (Chelli et al., 2017). The ecological regions or ecoregions have a relatively homogeneous ecological condition in which the evaluations and comparisons of biodiversity are meaningful within them (Painho et al., 1996). The digital map of European ecological regions (DMEER) employed herein is provided by European Environment Agency (2022). These ecoregions are delineated based on several factors, such as climate, topography, soil, geobotanical European data, and the assessment and judgment of a large team of experts from many European nature-related institutions and the World Wide Fund for Nature (WWF). Fig. 1 shows the ecoregions of Italy derived from DMEER and their topography. The background elevation in meters above the mean sea level shown in Fig. 1b is from the Shuttle Radar Topography Mission (SRTM) plus at ~30 m spatial resolution provided by Jet Propulsion Laboratory (Farr et al., 2007). Table 1 lists the names and areas of these ecoregions along with their climates, where the annual average precipitation for each ecoregion was estimated from the GPM observations during 2000–2021.

2.2. Datasets and pre-processing

The descriptions of data employed in this research can be found in Table 2. Image pre-processing, including sub-setting and geographic projection into the WGS84 (world geodetic system) coordinate system, is performed through Google Earth Engine (GEE) and Geographic Information System (GIS) platforms (QGIS). For Pearson correlation analysis and generating monthly maps, monthly NDVI data were produced from 16-day data using a weighted method as demonstrated in Figure 5 in Didan and Munoz (2019). For each ecoregion, a specific weight was assigned to each 16-day time series value which was the number of good-quality pixels divided by the total number of pixels within that ecoregion. Fig. 2 shows the weights associated with the ecoregion-based NDVI time series, categorized into four classes. The number of

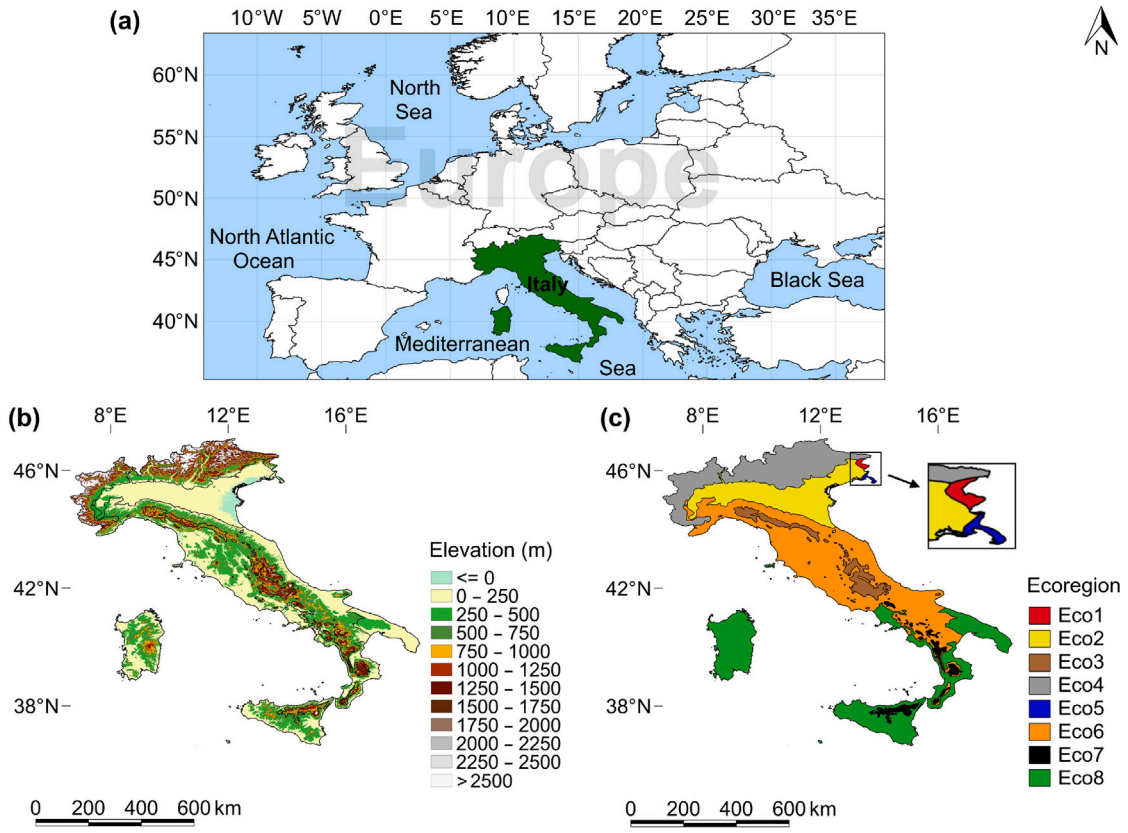

Fig. 1. (a) A map of Europe showing Italy in green, (b) the ecoregion boundaries in Italy overlaid on DEM-SRTM (30 m spatial resolution), and (c) the ecoregions of Italy. (For interpretation of the references to colour in this figure legend, the reader is referred to the web version of this article.)

Table 1
The ecoregions of Italy and their areas and climates, see Fig. 1c.

Label	Ecoregion's name	Area (km^2)	Annual average temperature (°C)	Annual average precipitation (mm)
Eco1	Dinaric mountains mixed forests	765.36	10 ± 7	1600 ± 300
Eco2	Po basin mixed forests	42 399.09	14 ± 9	1000 ± 200
Eco3	Apennine deciduous montane forests	14 600.95	10 ± 8	900 ± 200
Eco4	Alps conifer and mixed forests	52 124.46	6 ± 8	1100 ± 200
Eco5	Illyrian deciduous forests	514.88	13 ± 8	1400 ± 300
Eco6	Italian sclerophyllous and semi-deciduous forests	108 094.68	15 ± 8	800 ± 200
Eco7	South Apennine mixed montane forests	8248.03	13 ± 7	800 ± 300
Eco8	Tyrrhenian-Adriatic sclerophyllous and mixed forests	73 973.85	17 ± 8	700 ± 200

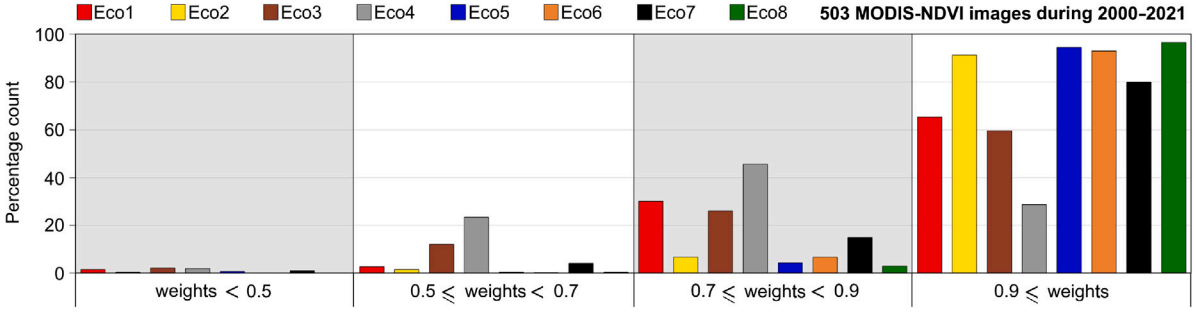

Fig. 2. Weight distributions of 16-day NDVI time series calculated for ecoregions of Italy.

observations whose weights fall in each class was counted to generate the bar charts. It shows that Eco3 and Eco4 have more uncertainties due to clouds than other ecoregions, e.g., more than 20% and 40% of the observations in the NDVI time series correspond to Eco4 have weights in the range of [0.5, 0.7) and [0.7, 0.9), respectively (see the grey bars in Fig. 2).

Table 2
Datasets used in this study with their properties.

Data	Date	Temporal resolution	Spatial resolution	No. images	Product name	Digital object identifier (DOI)
NDVI	2000–2021	16-day	250 m	503	MOD13Q1 V6.1	10.5067/MODIS/MOD13Q1.061
LST	2000–2021	Monthly	0.05° × 0.05°	263	MOD11C3 V6.1	10.5067/MODIS/MOD11C3.061
Precipitation	2000–2021	Monthly	0.1° × 0.1°	252	GPM V6	10.5067/GPM/IMERG/3B-MONTH/06
Land cover	2001–2020	Annually	500 m	20	MCD12Q1 V6	10.5067/MODIS/MCD12Q1.006
SRTM-plus	2000	February 2000	30 m	1	SRTMGL1N V3	10.5067/MEaSUREs/SRTM/SRTMGL1N.003

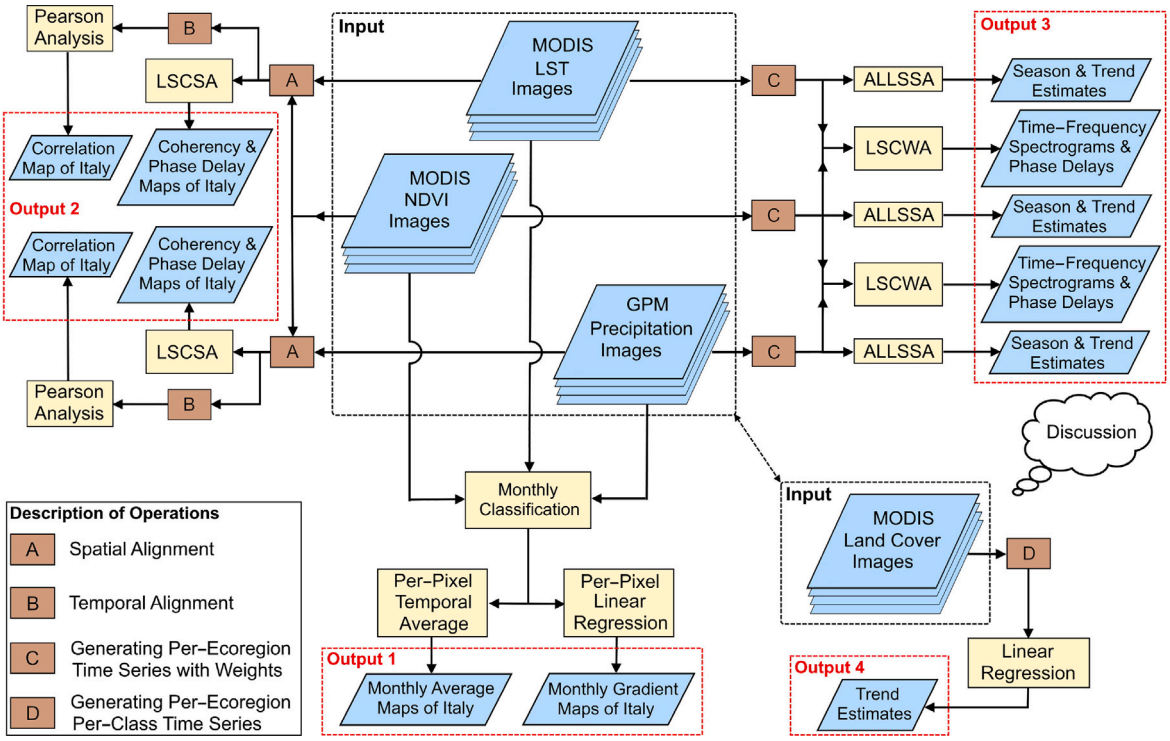

Fig. 3. The workflow of this study. (For interpretation of the references to colour in this figure legend, the reader is referred to the web version of this article.)

The monthly MODIS LST product consists of monthly cloud-free daytime and nighttime LST since February 2000. The MOD11C3 Version 6.1 is an improvement of former versions in that the LST is estimated based on various calibration processes, adjustment of the optical crosstalk in infrared bands, correction of the reflective solar bands, and others (Wan, 2014). Herein, in addition to analysing daytime and nighttime LST observations, the average of cloud-free daytime and nighttime monthly observations was calculated for each pixel as a proxy of overall monthly LSTs (Chen et al., 2017).

Monthly GPM level 3 data have been derived by inter-calibrating and interpolating all precipitation microwave and infrared satellite estimates, precipitation gauge analyses, and other precipitation estimators at fine time and space scales (Adler et al., 2018; Kidd, 2018). A rigorous precipitation gauge analysis, using global precipitation climatology centre (GPCC) products, has been performed for calibrating and correcting the biases from satellite precipitation estimates and to provide reliable monthly precipitation data (Schneider et al., 2014; Gehne et al., 2016). In this research, monthly merged satellite-gauge precipitation estimates and their random errors have been employed for correlation and coherency analyses. The period of record of monthly GPM data is from June 2000 to June 2021.

The MODIS land cover type product (MCD12Q1) is derived from a combination of Terra and Aqua MODIS data via a rigorous supervised classification scheme (Sulla-Menashe et al., 2019). MCD12Q1 has 11 classes: water bodies, grasslands, shrublands, broadleaf croplands, grassy woodlands (sparse trees), evergreen broadleaf forests, deciduous broadleaf forests, evergreen needleleaf forests, deciduous needleleaf forests, non-vegetated lands, and urban. For more details about these classes, see the user guide at https://doi.org/10.5067/MODIS/MCD12Q1.006.

2.3. Methods

The methods described here are applied to NDVI and climate datasets to produce four different sets of output as illustrated in Fig. 3. To obtain output 1, the images were grouped into the calendar months to generate monthly average and gradient maps using QGIS during 2000–2021, respectively. To obtain output 2, NDVI was spatially downsampled using a median approach to match the resolution of LST for per-pixel Pearson correlation and LSCSA annual coherency and phase delay analyses. Likewise, NDVI was spatially downsampled to match the resolution of precipitation for the analyses (operation A in Fig. 3). To obtain output 3, the ecoregion-based NDVI, LST, and precipitation time series were generated along with their statistical weights (see Fig. 2 and operation C in Fig. 3), also excluding water bodies from the analysis using the land cover water class. The ALLSSA was implemented to estimate season and trend simultaneously. The LSCSA and LSCWA were also performed for estimating the coherency and phase delay between cycles of the pairs of time series for each ecoregion. For comparison, Person correlation coefficient was also estimated for each pair of temporally aligned time series. To obtain output 4, the annual MODIS land cover data were utilized, and linear

regression was performed on each per-ecoregion per-class time series to investigate changes in land cover classes for each ecoregion since 2001 and their linkage with NDVI and climate.

Pearson correlation coefficient r is in range $[-1, 1]$. Values between 0 and 0.3 or 0 and -0.3 indicate a weak positive or weak negative correlation. Values between 0.3 and 0.7 or -0.3 and -0.7 indicate a moderately positive or negative fuzzy linear dependency while values between 0.7 and 1 or -0.7 and -1 show a strong positive or negative linear dependency between variables (Ratner, 2009). To estimate the correlation between multiple time series, the time series data must be first aligned in time, e.g., both time series be sampled monthly with no missing values (see operation B in Fig. 3). The LSCSA first decomposes each time series into a common frequency domain regardless of its time distribution. Then it calculates a least-squares cross-spectrum (LSCS) by multiplying the time series spectra which shows the coherent spectral peaks. The values of these peaks are expressed in percentage variance, where values greater than 25% indicate significant coherency between the estimated sinusoidal cycles of the same frequency (Ghaderpour et al., 2018). The LSCWA decomposes each time series into a time–frequency domain to obtain a least-squares cross-wavelet spectrogram (LSCWS) which shows the spectral peaks within localized time–frequency neighbourhoods. Like LSCS, the spectral peaks in LSCWS are expressed in percentage variance, but they are interpreted locally in time rather than globally. The Morlet wavelet with its default settings was used to calculate the cross-spectrograms in the LSWAVE software, creating optimal time–frequency resolution cross-spectrograms (Torrence and Compo, 1998; Ghaderpour et al., 2021). Spectral peaks can be suppressed/removed from LSCS or LSCWS to obtain a residual LSCS (RLSCS) or residual LSCWS (RLSCWS), respectively. This process is done globally in LSCSA but is done locally (segment-wise) in LSCWA. The stochastic surface in the LSCWS also shows whether a peak is significant at a confidence level (e.g., 99%). If the peak value is greater than the critical value, i.e., the peak stands above the stochastic surface, then the peak is statistically significant. The phase delays are typically portrayed by white arrows on the LSCWSs, following the principle of the trigonometric circle, see Ghaderpour et al. (2021) and Dastour et al. (2022) for more details.

3. Results

This section describes the results of analysing NDVI, LST, and precipitation data at both pixel and ecoregion levels. Lastly, the temporal and spatial dynamics of annual land cover data are presented for the sake of assessment and discussion. The ALLSSA results are shown for daytime, diurnal (average of daytime and nighttime), and nighttime LST. For brevity, the correlation and coherency results are illustrated only for diurnal LST (simply LST) as the results for daytime and nighttime LST were very similar to diurnal LST. Note that the subsection numbers here exactly refer to the output numbers shown in red in Fig. 3 to aid understanding.

3.1. Spatiotemporal maps of NDVI and climate across Italy

The monthly average geospatial maps of NDVI, LST, and precipitation across Italy during 2000–2021 are illustrated in Figs. A.1–A.3, respectively. Fig. A.1 shows that NDVI was relatively higher in summer but lower in winter for northern Italy while this relation was opposite for the southern Italy, including Sardinia. Fig. A.2 shows that Eco4 and Eco8 had relatively cooler and warmer months compared to other ecoregions, respectively. Fig. A.3 also shows that Eco8 was the driest ecoregion during summer.

The monthly gradient maps of NDVI, LST, and precipitation at 95% confidence level for Italy are displayed in Figs. A.4–A.6, respectively. These maps were generated by analysing per-pixel time series of sizes less than or equal to 22, depending on cloud contamination. The overall gradient for each per-pixel time series was estimated by the linear regression method. Only the statistically significant gradients at 95% are demonstrated here. Fig. 4 shows the bar charts for percentage counts of positive or negative NDVI gradients illustrated in Fig. A.4. Each bar, corresponding to a month and an ecoregion, is obtained by dividing the total number of pixels whose gradients were positive (negative) in that month by the total number of pixels in that ecoregion. From Fig. 4, one can observe that relatively much more areas have been greening since 2000 for all ecoregions. Fig. A.5 also shows that May has been cooling while September has been warming for some parts of all ecoregions, particularly for Eco2. Furthermore, only four months showed significant precipitation gradients, mostly in Eco6–Eco8 (see Fig. A.6).

3.2. Correlation, coherency, and phase delay maps between NDVI and climate

Fig. 5 shows the results of applying Pearson correlation and LSCSA to the spatially aligned NDVI and LST and spatially aligned NDVI and precipitation per-pixel time series. The LSCSA results are shown only for the annual cycles in the per-pixel time series that were mainly the most significant cycles in the time series. Comparing panel (b) with panel (e), one can observe that the annual percentage variance (coherency) for NDVI and LST was stronger (at least twice) than the annual percentage variance for NDVI and precipitation. Panels (c) shows the phase delay analysis between the annual cycles of NDVI and LST. Likewise, panels (f) shows the phase delay analysis between the annual cycles of NDVI and precipitation. Panel (a) shows that NDVI in most of Eco8 was negatively correlated with LST, and panel (c) shows that the annual cycles of NDVI and LST were almost out-of-phase for Eco8. Most of Eco6 and Eco7 had relatively much weaker annual coherency than the other ecoregions as can be seen in panel (b). The mountainous ecoregions Eco3 and Eco4 had the most positive correlation and annual coherency between NDVI and LST whose annual cycles were also approximately in-phase. As for the relationship between NDVI and precipitation, panels (d) and (e) show the lowest correlation and annual coherency for Eco2 (insignificant) while the highest correlation and annual coherency were for Eco8. Panel (f) shows that the annual cycle of precipitation led the annual cycle of NDVI by about one month for Eco8.

3.3. LSWAVE results of NDVI and climate for ecoregions

The 16-day NDVI and monthly LST and precipitation time series for the ecoregions are illustrated in Figs. A.7–A.11 and Fig. 6. The weights associated with the NDVI time series values were calculated based on the number of cloud-contaminated pixels in each ecoregion as demonstrated in Fig. 2. The weights for climate time series were also estimated from the random errors associated with the climate pixels. The simultaneous season-trend fit results using ALLSSA are listed in Tables A.1–A.3. The harmonics at higher estimated frequencies have lower amplitudes and omitting them do not significantly change the gradients. From Table A.1, all ecoregions have been slightly greening by 0.003 NDVI/year since 2000 with the highest annual amplitude ($\sim$0.22) estimated for Eco1 and Eco4. The ALLSSA estimated statistically significant annual, semi-annual, and four-monthly (3 cycles/year) cycles for all ecoregions.

Table A.2 shows that all ecoregions have been warming at different rates since 2000, except the daytime and diurnal LST for Eco7 and Eco8. Eco2 had the most significant overall positive diurnal LST trend among other Italian ecoregions (0.05 °C/year), where most of this change occurred during July and September (cf., Fig. A.5). In ALLSSA when the estimated error is greater than the magnitude of the estimated gradient, the gradient is insignificant, i.e., the linear trend cannot be used as predictor.

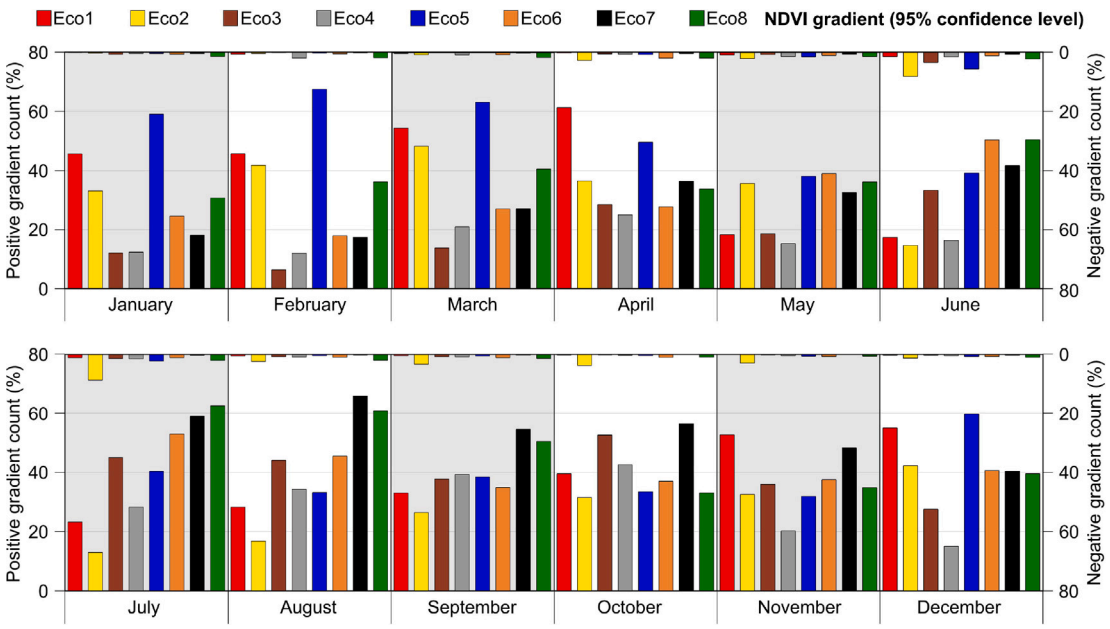

Fig. 4. The bar charts showing the percentage counts of statistically significant positive and negative NDVI gradients at 95% shown in Fig. A.4 for the ecoregions.

Table A.3 shows that precipitation has been slightly declining since 2000 for Eco3, Eco6, and Eco7. No statistically significant semi-annual cycle was estimated for Eco1, Eco4, and Eco5. Furthermore, Eco5 did not have any statistically significant annual cycle. Eco7 and Eco8 had the highest amplitude for the annual cycle (~36 mm).

For brevity, the LSCSA and LSCWA results are displayed for Eco8 in Fig. 6. The LSCSA and LSCWA results for other ecoregions are illustrated in Figs. A.8–A.11, where they are categorized based on climate and elevation of ecoregions to better aid comparison between ecoregions. Furthermore, Pearson correlation and LSCSA results for the ecoregion time series are summarized in Table 3. After the estimations of cross-spectra and cross-spectrograms, the annual peaks at 1 cycle/year were found to be the most dominant peaks, and so in the next step the annual peaks were removed from the cross-spectra and cross-spectrograms to obtain RLSCSs and RLSCWSs. In the cross-spectrograms, arrows pointing toward the positive and negative direction of the time axis mean the estimated harmonics are in-phase and out-of-phase, respectively. Arrows pointing toward the positive and negative direction of the frequency axis indicate that the estimated cycles in the NDVI time series lead and lag the ones in the LST time series by a quarter cycle (90 degrees), respectively. Furthermore, the grey surface is the stochastic surface at 99% confidence level (similarly for NDVI and precipitation). All the LSCWSs for the ecoregions share the same colour bar to aid visualization and comparison, similarly, unique colour bars were chosen for the RLSCWSs and stochastic surfaces.

Fig. 6a shows that NDVI and LST have significant annual coherency (~80%), see the horizontal coherent peaks at 1 cycle/year in the LSCWS. The direction of arrows for the annual peaks indicates that the annual cycles of NDVI and LST were out-of-phase since 2000, meaning warming had a reverse effect on greening and vice versa (see the white arrows displayed on the annual spectral peaks in LSCWS pointing toward the left). Fig. 6b also shows significant annual coherency between NDVI and precipitation which is more pronounced between 2010 to 2015. However, the direction of arrows (toward bottom-right) displayed on the LSCWS indicates that when the annual cycle of precipitation reached its maximum, about one month after the annual cycle of NDVI reached its maximum, and the annual cycle of LST reached its minimum about one month after the annual cycle of precipitation reached its minimum. After removing the annual coherent peaks, the RLSCWSs show seasonal cycles of NDVI and LST were coherent with phase discrepancy. Their coherency is more pronounced in certain periods. For example, semi-annual coherency of more than 30% was estimated between NDVI and LST in 2008 and 2010 while their semi-annual cycles were out-of-phase in these years, see the direction of the arrows displayed on the significant coherent peaks at 2 cycles/year in the RLSCWSs in Fig. 6a. Interestingly, in 2008 and 2010, the semi-annual cycles of NDVI and precipitation were in-phase and significantly coherent.

From the LSCWSs illustrated in Figs. A.8–A.11, one can observe that the annual cycles of NDVI and LST for Eco1–Eco5 were significantly coherent over time and almost in-phase which means annual warming and greening occurred at almost the same time; however, the annual cycles of NDVI led LST by a few weeks for Eco6 and Eco7 with relatively much lower coherency (less than 40%). The annual cycles of NDVI and precipitation were relatively much less coherent for Eco1–Eco7. Table 3 summarizes the LSCSA results for the annual cycles of NDVI and climate time series corresponding to each ecoregion. It can be seen that the correlation (0.53) and annual coherency (39%) between NDVI and precipitation are significant only for Eco8.

3.4. Temporal and spatial dynamics of land cover

The land cover maps for 2001, 2010, and 2020 are illustrated in Fig. A.12. The annual time series of land cover types for each ecoregion was obtained by counting the number of pixels for each land cover type within the ecoregion and dividing it by the total number of pixels in the ecoregion, Fig. A.13. The average of each time series, representing the percentage amount of a land cover type in an ecoregion, is listed in Table 4. In addition, linear regression was applied to estimate the slope of each time series. The estimated slopes along with their standard errors are also listed in Table 4, which show the amount of grasslands has been significantly declining for all ecoregions except Eco4 while the amount of grassy woodlands was increasing for all ecoregions at 95% confidence level.

4. Discussion

Table 3 showed that the annual cycles of LST led the ones in NDVI by a few days for Eco3 and Eco4, likewise for Eco1 and Eco5. The seasonal cycles of LST also led the ones in NDVI. This is mainly due to relatively cooler and wetter climate as well as their land cover types. Deciduous broadleaf forests, grasslands, and grassy woodlands

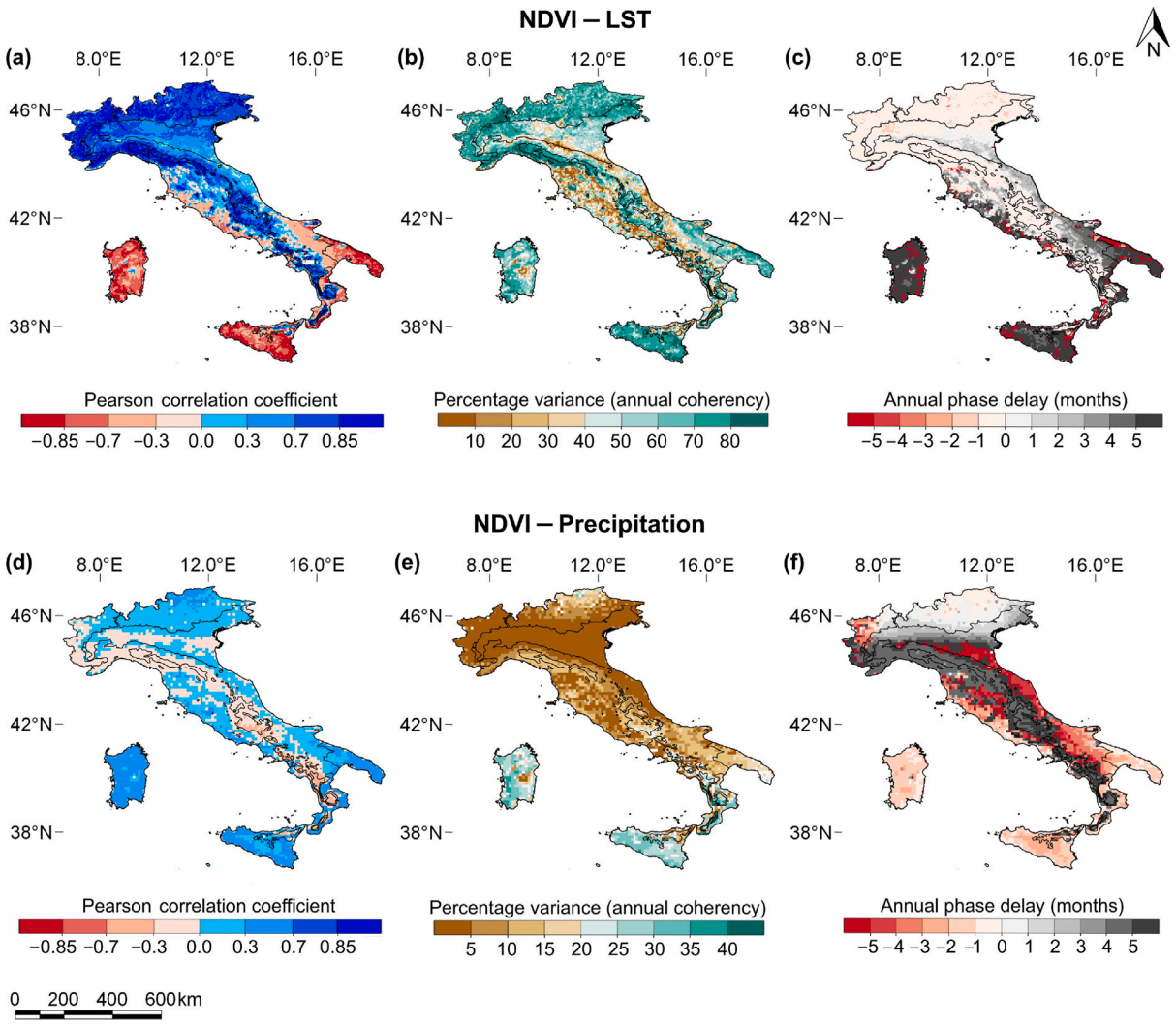

Fig. 5. Geospatial maps showing (a) the Pearson correlation, (b) annual coherency, (c) annual phase delay results for NDVI and LST time series at $0.05° \times 0.05°$ spatial resolution, (d) the Pearson correlation, (e) annual coherency, and (f) annual phase delay results for NDVI and precipitation time series at $0.1° \times 0.1°$ spatial resolution. The positive and negative values in panel (c) show how much the annual cycle of NDVI lead and lag the annual cycle of LST, respectively. Likewise, the positive and negative values in panel (f) show how much the annual cycle of NDVI lead and lag the annual cycle of precipitation, respectively. Panels (b), (c), (e), and (f) are obtained by applying the LSCSA to per-pixel time series.

Table 3
Statistical relations between NDVI and LST and between NDVI and precipitation time series for ecoregions of Italy using Pearson correlation analysis and LSCSA. Note that the positive and negative values in the fourth column mean that the annual cycle of NDVI lags and leads the annual cycle of LST, respectively (likewise for the NDVI and precipitation in the last column).

Ecoregions of Italy	NDVI-LST correlation r	NDVI-LST annual coherency (%)	NDVI-LST annual time delay (days)	NDVI-Precip correlation r	NDVI-Precip annual coherency (%)	NDVI-Precip annual time delay (days)
Eco1	0.91	85	−5	0.04	6	17
Eco2	0.85	71	5	0.04	2	31
Eco3	0.88	78	−3	−0.26	8	159
Eco4	0.92	85	−4	0.21	12	−2
Eco5	0.86	80	−6	−0.01	2	51
Eco6	0.52	34	34	0.00	4	−176
Eco7	0.62	37	16	−0.39	16	172
Eco8	−0.86	75	173	0.53	39	−31

are the major land cover types in these ecoregions (Figs. A.12 and A.13). Therefore, roughly speaking when the temperature reached its annual maximum, a few days after NDVI became maximum, and NDVI became minimum a few days after the annual temperature reached its minimum. A similar NDVI response to climate (2–3 weeks phase delay) was also reported for the Athabasca River Basin in Alberta Canada which has a cold climate with similar land cover types (Dastour et al., 2022). As illustrated in Fig. A.5, over 60% of Eco3 (Apennine deciduous montane forests) has been cooling in May without any significant changes in other months which may be explained by increasing the amount of grassy woodlands (sparse trees) and forests, see Table 4.

From Fig. A.5, parts of Eco2 were significantly warming in June, July, and September. Eco2 experienced overall warming of 0.05 °C per year, see Table A.2, where grasslands were significantly decreasing while grassy woodlands and urban were increasing during the past

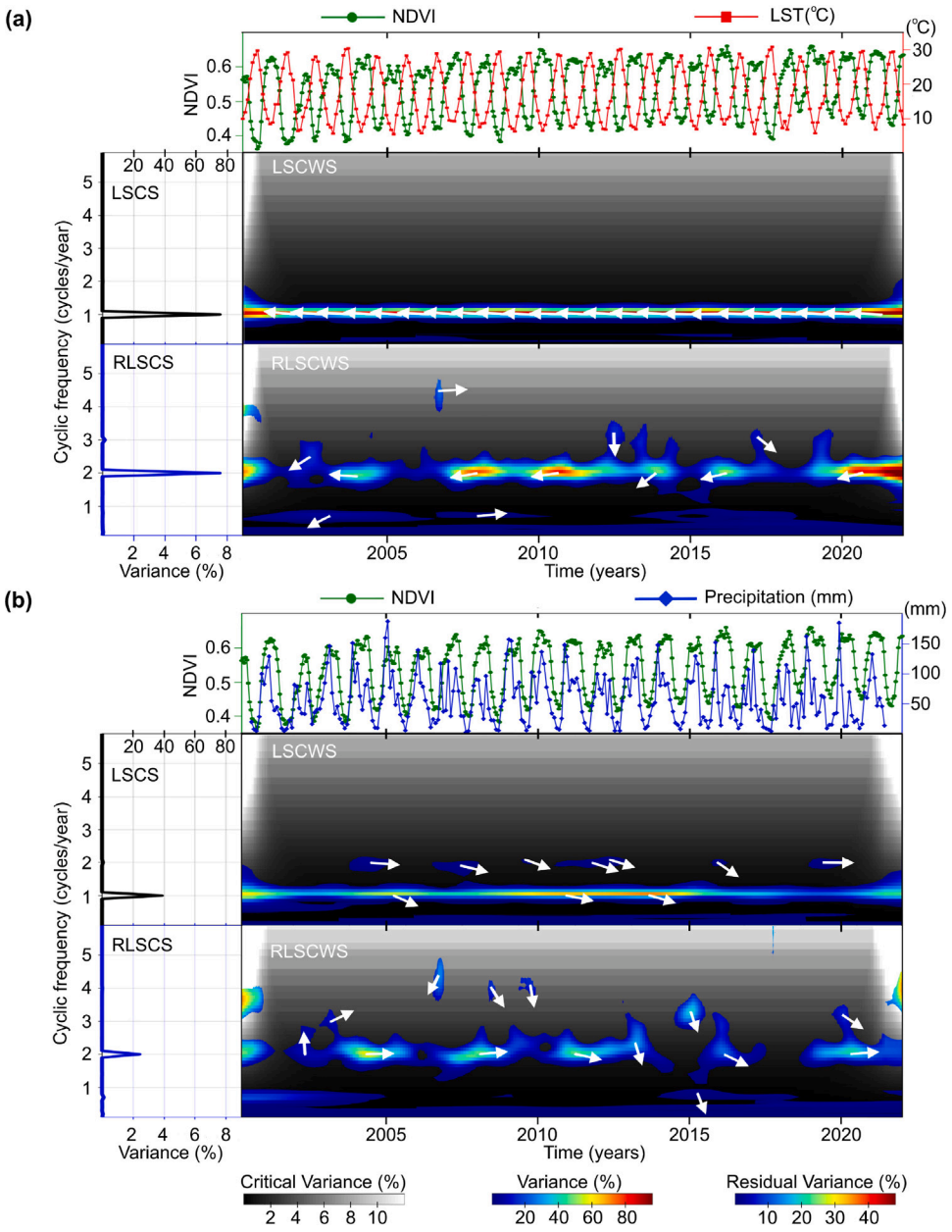

Fig. 6. The LSCSA and LSCWA results for (a) MODIS NDVI and LST time series, and (b) MODIS NDVI and GPM precipitation corresponding to Eco8. The grey surface overlaid on each cross-spectrogram is the stochastic surface at 99% confidence level. The arrows show the phase lead/lag. Arrows pointing to the right, left, top, and bottom mean the cycles are in-phase, out-of-phase, NDVI cycles lead and lag LST (precipitation) cycles, respectively. Note that RLSCS and RLSCWS are respectively the residual cross spectrum and cross-wavelet spectrogram, obtained after *removing* the annual cycles of NDVI, LST, and precipitation time series. (For interpretation of the references to colour in this figure legend, the reader is referred to the web version of this article.)

two decades in this ecoregion, see Table 4. These natural or artificial land cover dynamics (e.g., due to fire, urbanization, industrial activities) may explain the significant warming trend observed in this ecoregion. Zullo et al. (2019) investigated the effect of urban growth on LST in this ecoregion and found that in daytime and diurnal conditions, LST has increased by ~1.36 °C and ~0.93 °C during 2001–2011, respectively, which agrees with the findings of this research. Anniballe et al. (2014) highlighted the potential influence of existing plants and green areas in built-up areas in this ecoregion for reducing the urban heat island. Warming, reduction of riverine vegetation, and urban and agricultural pollutions seem to have a negative impact on the biodiversity and ecosystem of the ecoregion, including fish species along the Po River in recent years (Castaldelli et al., 2013).

As observed in Fig. 5b, most parts of Eco6 and Eco7 showed relatively much lower annual coherency, particularly in Tuscany, meaning that the annual temperature variation was less coherent with the annual vegetation dynamic, see also Table 3. This behaviour may be explained by climatic conditions, diversified growing cycles, and human-induced factors, such as irrigation (Maselli et al., 2020). Due to relatively lower annual precipitation in Eco8, as shown in Table 1, vegetation including grasslands, grassy woodlands, and broadleaf croplands was more in stress during hot and dry summers, which could explain why the annual and seasonal cycles of NDVI and LST were out-of-phase in Eco8 (Piao et al., 2014). The in-phase annual cycles of NDVI and precipitation, demonstrated in Fig. 6, indicate the importance of precipitation for cooling and greening in Eco8. Other potential contributing factors to such NDVI dynamics could be albedo, surface resistance to evapotranspiration, and seasonal irrigation (Zhang et al., 2008). This vegetation response to climate also conforms with Capodici et al. (2020) who noticed a strong negative correlation between LST and NDVI for the

Table 4
The estimated averages and gradients for land cover types using linear regression. The first and second rows for each land cover type show the average percentage area coverage and the estimated gradient (percentage per year) for the ecoregions of Italy during 2001–2020, respectively. The highlighted numbers also show the most significant gradients for each land cover type. The land cover types 'Water bodies', 'Shrublands', and 'Deciduous Needleleaf Forests' are not listed here because they were insignificant in all ecoregions.

Land cover type	Eco1	Eco2	Eco3	Eco4	Eco5	Eco6	Eco7	Eco8
Grasslands	11.75 ± 1.23	71.71 ± 2.17	23.98 ± 2.16	25.60 ± 0.42	11.11 ± 1.27	34.78 ± 2.97	28.72 ± 2.14	43.79 ± 1.63
	−0.19 ± 0.02*	−0.35 ± 0.03*	−0.34 ± 0.03*	0.01 ± 0.02	−0.16 ± 0.03*	−0.48 ± 0.04*	−0.35 ± 0.02*	−0.26 ± 0.02*
Broadleaf Croplands	0.08 ± 0.03	6.72 ± 0.60	0.02 ± 0.01	1.38 ± 0.11	12.21 ± 0.51	5.98 ± 0.43	0.81 ± 0.10	12.70 ± 0.54
	0.00 ± 0.00	0.08 ± 0.01*	0.00 ± 0.00*	−0.01 ± 0.00*	−0.08 ± 0.01*	−0.05 ± 0.01*	0.00 ± 0.00	0.00 ± 0.02
Grassy Woodlands	17.19 ± 2.16	7.25 ± 1.62	41.34 ± 1.58	29.47 ± 0.94	31.09 ± 3.82	42.42 ± 2.74	42.17 ± 1.00	27.62 ± 1.11
	0.35 ± 0.02*	0.26 ± 0.02*	0.25 ± 0.02*	0.08 ± 0.03*	0.55 ± 0.08*	0.45 ± 0.02*	0.16 ± 0.02*	0.15 ± 0.03*
Evergreen Broadleaf	0.00 ± 0.00	0.00 ± 0.00	0.12 ± 0.01	0.00 ± 0.00	0.04 ± 0.03	1.82 ± 0.04	1.21 ± 0.07	3.34 ± 0.34
	0.00 ± 0.00	0.00 ± 0.00	0.00 ± 0.00*	0.00 ± 0.00	0.00 ± 0.00*	0.00 ± 0.00	0.01 ± 0.00*	0.04 ± 0.01*
Deciduous Broadleaf	66.36 ± 1.21	1.57 ± 0.07	33.70 ± 1.20	21.40 ± 0.99	22.58 ± 2.23	9.96 ± 0.54	21.10 ± 0.76	1.61 ± 0.12
	−0.20 ± 0.01*	−0.01 ± 0.00*	0.08 ± 0.04	−0.07 ± 0.04*	−0.31 ± 0.05*	0.06 ± 0.02*	0.11 ± 0.01*	0.01 ± 0.00*
Evergreen Needleleaf	3.23 ± 0.24	0.08 ± 0.01	0.66 ± 0.09	13.99 ± 0.25	0.62 ± 0.07	1.36 ± 0.13	4.28 ± 0.52	4.75 ± 0.54
	0.03 ± 0.01*	0.00 ± 0.00*	0.01 ± 0.00*	0.01 ± 0.01	0.00 ± 0.00	0.02 ± 0.00*	0.09 ± 0.00*	0.06 ± 0.02*
Non-Vegetated	0.51 ± 0.07	0.01 ± 0.00	0.01 ± 0.01	3.54 ± 0.15	0.48 ± 0.00	0.01 ± 0.00	1.03 ± 0.03	0.06 ± 0.01
	0.00 ± 0.00	0.00 ± 0.00*	0.00 ± 0.00*	−0.02 ± 0.00*	0.00 ± 0.00*	0.00 ± 0.00*	0.00 ± 0.00*	0.00 ± 0.00*
Urban	0.88 ± 0.00	11.42 ± 0.10	0.13 ± 0.00	3.49 ± 0.01	19.55 ± 0.02	3.15 ± 0.01	0.43 ± 0.00	5.68 ± 0.02
	0.00 ± 0.00*	0.02 ± 0.00*	0.00 ± 0.00*	0.00 ± 0.00*	0.00 ± 0.00*	0.00 ± 0.00*	0.00 ± 0.00	0.00 ± 0.00*

*Symbol means that the estimated gradient is statistically significant at 95% confidence level.

Imera Meridionale basin in Sicily, a part of Eco8. It also agrees with the findings of Lai et al. (2020) who pointed out that NDVI and LST were negatively correlated in Sardinia, noting that almost half of the regional land in Sardinia is agricultural land (e.g., broadleaf cropland) where vegetation growth is strongly depended on precipitation. From Table 4, a slight increase in broadleaf and needleleaf forests in Eco7 and Eco8 was likely a contributing factor to daytime cooling of these ecoregions, though not significant (see Table A.2).

Fig. 4 showed that relatively larger parts of ecoregions have been greening in each month since 2000. The LSWAVE results in Table A.1 also showed that all ecoregions have been greening by 0.03 per decade. On the other hand, Table 4 and Fig. A.13 showed that within each ecoregion (excluding Eco4), most grasslands dominated by herbaceous annuals have been replacing by grassy woodlands and/or forests. Anthropogenic activities have had a significant influence on forest distribution in Apennine regions, i.e., abandonment of rural, traditional farming or grazing activities have resulted in forest expansion (Vacchiano et al., 2017). Afforestation has been occurring over the past few decades across Italy, especially on the Alps and Apennines ranges (Cavalli et al., 2022). The trend results for MODIS land cover types shown in Table 4 were also in agreement with the dynamics of the Italian land use inventory (IUTI) classes over the past two decades (Sallustio et al., 2016). Therefore, the gradual increase in forest coverage may explain the positive NDVI gradients in these ecoregions over the past two decades. Despite the moderate resolution of MODIS imagery, uncontrolled vegetation growth can still be monitored through vegetation indices which can help in detecting and managing areas that are susceptible to destruction due to fires and their consequences, such as floods and landslides.

The RLSCWSs in Figs. A.8–A.11 and Fig. 6 showed that semi-annual cycles (2 cycles/year) of NDVI and LST were more coherent for Eco6, Eco7, and Eco8 than other ecoregions (more than 6% coherency), particularly in 2008 and 2010, but they were mostly out-of-phase, meaning that warming resulted in lowering NDVI and cooling resulted in increasing NDVI. Interestingly, the semi-annual cycles of the NDVI and precipitations were almost in-phase for Eco6, Eco7, and Eco8. The coherent peaks at 3 cycles/year with approximately 90 degrees or one-month phase delay were also detected for Eco1, Eco3, Eco4, and Eco5 which were more significant in 2015. Note that RLSCSs illustrated on the left sides of RLSCWSs do not show how these seasonal cycles are coherent over time.

While the analyses presented here carefully considered the observational uncertainties provided by the quality assurance bands in the MODIS products, it should be noted that still there exist issues in the MODIS products and cloud detection algorithms utilized by scientists and programmers to produce quality assurance bands (Stillinger et al., 2019; Qiu et al., 2020). Therefore, the results presented here should be interpreted with caution, particularly for the mountainous regions Eco3 and Eco4 which have high observational uncertainties, see Figs. 1 and 2. In addition to climate change, anthropogenic activities, such as deforestation, urbanization, industrial activities, and human-caused fires are also key factors affecting vegetation change. Investigating the impact of such activities on vegetation change is also very important and is subject to future research.

5. Conclusions

In this research, the advanced techniques in the LSWAVE software for frequency and time–frequency analyses of unequally sampled data were presented and applied to MODIS and GPM data since 2000 for Italy. Gradual changes in NDVI, LST, and precipitation were investigated for each calendar month at pixel levels. The ALLSSA season-trend fit model was also utilized to simultaneously estimate trends and harmonics of NDVI, LST (daytime, diurnal, nighttime), and precipitation time series for each ecoregion in Italy. Pearson correlation and LSCSA were applied to spatially aligned NDVI and climate data across Italy, and their results were compared. Pearson correlation method, LSCSA, and LSCWA were also applied to NDVI, LST, and precipitation time series for each ecoregion in Italy. While Pearson correlation method required the time series to be first aggregated and aligned in time, the LSCSA and LSCWA did not need such pre-processing and were directly applied to the time series with their original temporal resolutions. Unlike Pearson correlation, LSCSA and LSCWA estimated how the periodic/aperiodic components are coherent and how much they lead/lag. The LSWAVE tools considered the statistical weights for the time series values to estimate more accurately the trends and harmonic components of the time series. In addition, trends between MODIS land cover types were estimated for each Italian ecoregion to discuss their interconnections with NDVI and climate dynamics. Some of the main results of this research are summarized below.

It was found that Po Basin mixed forest (Eco2), one of the most industrialized ecoregions in Italy and Europe, has been warming by 0.5 °C/decade particularly in July and September while no significant temperature gradients were estimated for the southern ecoregions Eco7 and Eco8. All ecoregions exhibited a significant coherency between annual cycles of NDVI and LST, with less than 40% for Eco6 and Eco7

and more than 70% for other ecoregions. The annual and semi-annual cycles of NDVI and LST were out-of-phase for Eco8, i.e., temperature and vegetation cycles lagged or led each other by about 180 degrees, while Eco1–Eco5 had approximately in-phase coherent annual cycles. Furthermore, the highest and the lowest annual coherencies between NDVI and precipitation were observed for Eco2 (2%) and Eco8 (39%), respectively. The correlation and coherency between NDVI and LST was generally much higher than the ones between NDVI and precipitation for all ecoregions. Relatively, more areas in all ecoregions showed statistically significant positive NDVI gradients for each month since 2000 which could potentially be due to afforestation/forest expansion in recent decades. It was shown that the forested regions with higher altitudes had positive correlation with almost in-phase annual coherency between NDVI and precipitation while vegetation in the warmest ecoregion (Eco8) was positively correlated with precipitation but negatively correlated with LST.

Gradual warming and declining annual precipitation in Italy, likely to continue by mid-century, may potentially increase the frequency of heavy precipitation events that can cause thread to electricity networks in flood-prone areas, increase flood risk and rainfall-induced landslides, and others. On the other hand, increased woodlands and climate change can increase the frequency of wildfire events and possibly post-fire mudslides. Gradual warming also affects energy demand by increasing cooling degree days during the summer. Therefore, developments of national climate change adaptation strategies as well as land and hazard management strategies become a crucial task. The findings of this study can be considered as a guide for agronomists, hazard management personnel, politicians, and stakeholders, and it can also be used for improving the ecological region boundaries in Italy and around the globe.

CRediT authorship contribution statement

Ebrahim Ghaderpour: Conceptualization, Formal analysis, Methodology, Writing – original draft. **Paolo Mazzanti:** Conceptualization, Methodology, Writing – review & editing. **Gabriele Scarascia Mugnozza:** Conceptualization, Methodology, Writing – review & editing. **Francesca Bozzano:** Conceptualization, Methodology, Writing – review & editing.

Declaration of competing interest

The authors declare that they have no known competing financial interests or personal relationships that could have appeared to influence the work reported in this paper.

Data availability

The MODIS and GPM data employed in this research are publicly available.

Acknowledgements

The authors thank NASA scientists and personnel for providing the satellite data used in this research. Special thanks to Drs. Giuseppe Scarascia Mugnozza, Quazi K. Hassan, Spiros D. Pagiatakis and reviewers for their careful review and constructive suggestions that greatly helped to improve the presentation of this paper. This research was financially supported by CERI Research Centre at the Sapienza University of Rome.

Appendix A. Supplementary data

Supplementary material related to this article can be found online at https://doi.org/10.1016/j.jag.2023.103241.

References

Abdulmana, S., Lim, A., Wongsai, S., et al., 2021. Land surface temperature and vegetation cover changes and their relationships in Taiwan from 2000 to 2020. Remote Sens. Appl. Soc. Environ. 24, 100636.

Adler, R.F., Sapiano, M.R.P., Huffman, G.J., et al., 2018. The global precipitation climatology project (GPCP) monthly analysis (new version 2.3) and a review of 2017 global precipitation. Atmosphere 9 (4), 138.

Alexander, C., 2021. Influence of the proportion, height and proximity of vegetation and buildings on urban land surface temperature. Int. J. Appl. Earth Obs. Geoinf. 95, 102265.

Anniballe, R., Bonafoni, S., Pichierri, M., 2014. Spatial and temporal trends of the surface and air heat island over Milan using MODIS data. Remote Sens. Environ. 150, 163–171.

Capodici, F., Cammalleri, C., Francipane, et al., 2020. Soil water content diachronic mapping: An FFT frequency analysis of a temperature–Vegetation index. Geosciences 10 (1), 23.

Castaldelli, G., Pluchinotta, A., Milardi, M., et al., 2013. Introduction of exotic fish species and decline of native species in the lower Po basin, north-eastern Italy. Aquat. Conserv.: Mar. Freshw. Ecosyst. 23 (3), 405–417.

Cavalli, A., Francini, S., Cecili, G., et al., 2022. Afforestation monitoring through automatic analysis of 36-years Landsat Best Available Composites. IForest 15 (4), 220–228.

Chelli, S., Wellstein, C., Campetella, G., et al., 2017. Climate change response of vegetation across climatic zones in Italy. Clim. Res. 71 (3), 249–262.

Chen, X., Su, Z., Ma, Y., et al., 2017. An accurate estimate of monthly mean land surface temperatures from MODIS clear-sky retrievals. J. Hydrometeorol. 18 (10), 2827–2847.

Dastour, H., Ghaderpour, E., Zaghloul, M.S., et al., 2022. Wavelet-based spatiotemporal analyses of climate and vegetation for the Athabasca river basin in Canada. Int. J. Appl. Earth Obs. Geoinf. 114, 103044.

Deng, Y., Wang, S., Bai, X., et al., 2018. Relationship among land surface temperature and LUCC, NDVI in typical karst area. Sci. Rep. 8, 641.

Didan, K., Munoz, A.B., 2019. MODIS vegetation index user's guide (MOD13 series). Last update 2019. https://lpdacc.usgs.gov/documents/621/MOD13_User_Guide_V61.pdf.

European Environment Agency, 2022. Digital map of European ecological regions. https://www.eea.europa.eu/data-and-maps/data/digital-map-of-european-ecological-regions Accessed 6 2022.

Farr, T.G., et al., 2007. The shuttle radar topography mission. Rev. Geophys. 45 (2), RG2004. http://dx.doi.org/10.1029/2005RG000183.

Forzieri, G., Dakos, V., McDowell, N.G., et al., 2022. Emerging signals of declining forest resilience under climate change. Nature 608, 534–539.

Gehne, M., Hamill, T.M., Kiladis, G.N., et al., 2016. Comparison of global precipitation estimates across a range of temporal and spatial scales. J. Clim. 29 (21), 7773–7795.

Ghaderpour, E., 2021. JUST: MATLAB and python software for change detection and time series analysis. GPS Solut. 25 (85).

Ghaderpour, E., Ince, E.S., Pagiatakis, S.D., 2018. Least-squares cross-wavelet analysis and its applications in geophysical time series. J. Geod. 92, 1223–1236.

Ghaderpour, E., Pagiatakis, S.D., 2019. LSWAVE: a MATLAB software for the least-squares wavelet and cross-wavelet analyses. GPS Solut. 23 (50).

Ghaderpour, E., Vujadinovic, T., Hassan, Q.K., 2021. Application of the Least-Squares Wavelet software in hydrology: Athabasca River Basin. J. Hydrol. Reg. Stud. 36, 100847.

Ghorbanian, A., Mohammadzadeh, A., Jamali, S., 2022. Linear and non-linear vegetation trend analysis throughout Iran using two decades of MODIS NDVI imagery. Remote Sens. 14 (15), 3683.

Huffman, G.J., Bolvin, D.T., Braithwaite, D., Hsu, K., Joyce, R., 2017. NASA Global Precipitation Measurement (GPM) Integrated Multi-SatellitE Retrievals for GPM. IMERG, NASA Goddard Earth Sciences Data and Information Services Center, Greenbelt, MD, USA.

Kidd, C., 2018. Algorithm Theoretical Basis Document (ATBD) Version 01-02 for the NASA Global Precipitation Measurement (GPM) Precipitation Retrieval and Profiling Scheme (PRPS). GPM Project. Greenbelt, MD, p. 16, https://pps.gsfc.nasa.gov/Documents/20180203_SAPHIR-ATBD.pdf.

Lai, S., Leone, F., Zoppi, C., 2020. Spatial distribution of surface temperature and land cover: A study concerning sardinia, Italy. Sustainability 12 (8), 3186.

Lee Rodgers, J., Nicewander, W.A., 1988. Thirteen ways to look at the correlation coefficient. Am. Stat. 42 (1), 59–66.

Lian, X., Jiao, L., Liu, Z., et al., 2022. Multi-spatiotemporal heterogeneous legacy effects of climate on terrestrial vegetation dynamics in China. GIsci. Remote Sens. 59 (1), 164–183.

Mahmoud, M.T., Al-Zahrani, M.A., Sharif, H.O., 2018. Assessment of global precipitation measurement satellite products over Saudi Arabia. J. Hydrol. 559, 1–12.

Maselli, F., Angeli, L., Battista, P., et al., 2020. Evaluation of Terra/Aqua MODIS and Sentinel-2 MSI NDVI data for predicting actual evapotranspiration in Mediterranean regions. Int. J. Remote Sens. 41 (14), 5186–5205.

Moreira, A., Fontana, D.C., Kuplich, T.M., 2019. Wavelet approach applied to EVI/MODIS time series and meteorological data. ISPRS J. Photogramm. Remote Sens. 147, 335–344.
Neinavaz, E., Skidmore, A.K., Darvishzadeh, R., 2020. Effects of prediction accuracy of the proportion of vegetation cover on land surface emissivity and temperature using the NDVI threshold method. Int. J. Appl. Earth Obs. Geoinf. 85, 101984.
Painho, M., et al., 1996. Digital map of European ecological regions (DMEER): its concept and elaboration. In: Second Joint European Conference (JEC) & Exhibition on Geographical Information. Barcelona.
Piao, S., Nan, H., Huntingford, C., et al., 2014. Evidence for a weakening relationship between interannual temperature variability and northern vegetation activity. Nat. Commun. 5 (5018).
Qiu, S., Zhu, Z., Woodcock, C.E., 2020. Cirrus clouds that adversely affect Landsat 8 images: What are they and how to detect them? Remote Sens. Environ. 246, 111884.
Ratner, B., 2009. The correlation coefficient: Its values range between +1/–1, or do they? J. Target. Meas. Anal. Mark. 17, 139–142.
Sallustio, L., Munafò, M., Riitano, N., et al., 2016. Integration of land use and land cover inventories for landscape management and planning in Italy. Environ. Monit. Assess. 188, 1–20.
Sarvia, F., De Petris, S., Borgogno-Mondino, E., 2021. Exploring climate change effects on vegetation phenology by MOD13q1 data: The piemonte region case study in the period 2001–2019. Agronomy 11 (3), 555.
Schneider, U., Becker, A., Finger, P., et al., 2014. GPCC's new land-surface precipitation climatology based on quality-controlled in-situ data and its role in quantifying the global water cycle. Theor. Appl. Climatol. 115, 15–40.
Sciortino, M., De Felice, M., De Cecco, L., et al., 2020. Remote sensing for monitoring and mapping Land Productivity in Italy: A rapid assessment methodology. Catena 188, 104375.
Shawky, M., Ahmed, M.R., Ghaderpour, E., et al., 2023. Remote sensing-derived land surface temperature trends over South Asia. Ecol. Inf. 74, 101969.
Shawky, M., Moussa, A., Hassan, Q.K., et al., 2019. Performance assessment of sub-daily and daily precipitation estimates derived from GPM and GSMaP products over an arid environment. Remote Sens. 11 (23), 2840.
Skofronick-Jackson, G., Petersen, W.A., Berg, W., et al., 2017. The global precipitation measurement (GPM) mission for science and society. Bull. Am. Meteorol. Soc. 98 (8), 1679–1695.
Son, N.T., Chen, C.F., Chen, C.R., et al., 2012. Monitoring agricultural drought in the Lower Mekong Basin using MODIS NDVI and land surface temperature data. Int. J. Appl. Earth Obs. Geoinf. 18, 417–427.
Song, Z., Yang, H., Huang, X., et al., 2021. The spatiotemporal pattern and influencing factors of land surface temperature change in China from 2003 to 2019. Int. J. Appl. Earth Obs. Geoinf. 104, 102537.
Stillinger, T., Roberts, D.A., Collar, N.M., et al., 2019. Cloud masking for landsat 8 and MODIS terra over snow-covered terrain: Error analysis and spectral similarity between snow and cloud. Water Resour. Res. 55 (7), 6169–6184.
Sulla-Menashe, D., Gray, J.M., Abercrombie, S.P., et al., 2019. Hierarchical mapping of annual global land cover 2001 to present: The MODIS Collection 6 Land Cover product. Remote Sens. Environ. 222, 183–194.
Tomlinson, C.J., Chapman, L., Thornes, J.E., et al., 2011. Remote sensing land surface temperature for meteorology and climatology: a review. Met. Apps. 18 (3), 296–306.
Torrence, C., Compo, G.P., 1998. A practical guide to wavelet analysis. Bull. Am. Meteorol. Soc. 79 (1), 61–78.
Touhami, I., Moutahir, H., Assoul, D., et al., 2022. Multi-year monitoring land surface phenology in relation to climatic variables using MODIS-NDVI time-series in Mediterranean forest, Northeast Tunisia. Acta Oecologica 114, 103804.
Vacchiano, G., Garbarino, M., Lingua, E., et al., 2017. Forest dynamics and disturbance regimes in the Italian Apennines. For. Ecol. Manag. 388, 57–66.
Wan, Z., 2014. New refinements and validation of the Collection-6 MODIS land-surface temperature/emissivity products. Remote Sens. Environ. 140, 36–45.
Wang, J., Xie, Y., Wang, X., et al., 2019. Detecting patterns of vegetation gradual changes (2001–2017) in shiyang river basin, based on a novel framework. Remote Sens. 11 (21), 2475.
Yan, Y., Mao, K., Shi, J., et al., 2020. Driving forces of land surface temperature anomalous changes in North America in 2002–2018. Sci. Rep. 10, 6932.
Zhang, Y., Song, C., Band, L.E., et al., 2017. Reanalysis of global terrestrial vegetation trends from MODIS products: Browning or greening? Remote Sens. Environ. 191, 145–155.
Zhang, R., Tian, J., Su, H., et al., 2008. Two improvements of an operational two-layer model for terrestrial surface heat flux retrieval. Sensors 8 (10), 6165–6187.
Zullo, F., Fazio, G., Romano, B., et al., 2019. Effects of urban growth spatial pattern (UGSP) on the land surface temperature (LST): A study in the Po Valley (Italy). Sci. Total Environ. 650, 1740–1751.